
THE LIFECYCLE PRINCIPLE: STABILIZING DYNAMIC NEURAL NETWORKS WITH STATE MEMORY

Zichuan Yang

School of Mathematical Sciences
Tongji University
Shanghai, 200092, China
2153747@tongji.edu.cn

ABSTRACT

I investigate a stronger form of regularization by deactivating neurons for extended periods, a departure from the temporary changes of methods like Dropout. However, this long-term dynamism introduces a critical challenge: severe training instability when neurons are revived with random weights. To solve this, I propose the Lifecycle (LC) principle, a regularization mechanism centered on a key innovation: state memory. Instead of re-initializing a revived neuron, my method restores its parameters to their last known effective state. This process preserves learned knowledge and avoids destructive optimization shocks. My theoretical analysis reveals that the LC principle smooths the loss landscape, guiding optimization towards flatter minima associated with better generalization. Experiments on image classification benchmarks demonstrate that my method improves generalization and robustness. Crucially, ablation studies confirm that state memory is essential for achieving these gains.

1 INTRODUCTION

Biological systems, like the human brain, are not static. They constantly adapt through processes like apoptosis, where cells are pruned, and neurogenesis, where new connections are formed. This dynamic nature is crucial for learning and robustness. Inspired by this, I explored how to create a similar dynamic process inside an artificial neural network. My goal was to develop a new form of regularization.

Existing methods like Dropout introduce temporary changes to the network at each training step (Srivastava et al., 2014). This led me to a core question: what if these changes were not temporary, but lasted for longer periods? A mechanism that deactivates neurons for many epochs could force the network to build more robust and redundant representations. This is the central motivation for my work.

However, this idea presents a significant challenge. A long-term deactivation mechanism can severely disrupt the optimization process. If a neuron is deactivated and later re-initialized with random weights, it introduces a large, abrupt shock to the network. My initial experiments confirmed this. Such a process leads to highly unstable training and poor performance. The network struggles to adapt to these sudden, destructive changes. This observation revealed a core problem: long-term dynamism requires a stable revival mechanism.

To solve this stability problem, I propose the **Lifecycle (LC) principle**. The key component of this principle is **state memory**. This is my main contribution. Instead of re-initializing a revived neuron, my method restores its weights and bias to the values they had at the moment of deactivation. This memory-aware revival allows the neuron to re-integrate smoothly. It preserves the useful knowledge the neuron had previously learned. This avoids the destructive shock of random re-initialization. I also introduce a warm-up phase to further soften this re-integration.

My theoretical analysis suggests that the LC principle acts as a smoothing regularizer on the loss landscape. This encourages the optimizer to find flatter minima, which are often associated with bet-

ter generalization (Keskar et al., 2017). My analysis also connects the LC mechanism to a reduction in model capacity, providing a link to formal generalization bounds.

I evaluate my method on standard image classification benchmarks. I compare it against baseline models and other common regularization techniques. My experimental results show that the Life-cycle principle can improve generalization and robustness. The results also include ablation studies. These studies confirm the critical role of the state memory component for achieving stable and effective training. The remainder of this paper is organized as follows: Section 2 reviews related work. Section 3 details the methodology. Section 4 describes the experimental setup. Section 5 conducts theoretical analysis, and Section 6 concludes the paper.

2 RELATED WORK

My work is related to several areas of neural network research. These areas include stochastic regularization, network pruning, dynamic sparse training, and network growth. I will discuss each of these areas to precisely position my contribution.

2.1 STOCHASTIC REGULARIZATION

Dropout randomly sets neuron activations to zero during training to prevent co-adaptation (Srivastava et al., 2014). DropConnect is a similar method that sets individual weights to zero (Wan et al., 2013). These methods apply changes that are temporary and memoryless. The network structure is only altered for a single forward and backward pass. My Lifecycle principle is different. It introduces structural changes that are long-term. A neuron remains inactive for many epochs. This provides a different and potentially stronger regularization signal.

2.2 NETWORK PRUNING

Network pruning aims to reduce model size and improve efficiency. Pruning methods permanently remove unimportant weights or neurons from a trained network (Han et al., 2015; Blalock et al., 2020). The goal of pruning is typically model compression, not regularization. The removal of parameters is permanent. In contrast, my LC mechanism is designed for regularization. The deactivation of neurons is temporary, and they can be revived later in the training process.

2.3 DYNAMIC SPARSE TRAINING

Dynamic Sparse Training (DST) methods are perhaps the most related to my work. These methods change the network’s sparse connectivity during training. For example, SET prunes and randomly adds new connections in each epoch (Mocanu et al., 2018). RigL uses gradient information to decide which new connections to grow (Evci et al., 2020). These methods explore different sparse subnetworks. However, a key difference exists. When DST methods grow new connections, they are typically initialized to zero or small random values. This can introduce instability, as the network must learn these new parameters from scratch. My work directly addresses this specific problem. The Lifecycle principle operates at the neuron level, not the connection level. Most importantly, my core contribution of state memory ensures that a revived neuron is not re-initialized. It is restored to its last known effective state. This design choice is a direct solution to the optimization challenge that arises from abrupt structural changes in dynamic networks.

2.4 NETWORK GROWTH AND NEUROGENESIS

Another related area is network growth, sometimes referred to as neurogenesis. These methods start with a small network and dynamically add new neurons or layers during training. For example, Net2Net can instantly make a network wider or deeper while preserving its function (Chen et al., 2015). Other methods, like Dynamically Expandable Networks (DEN) add neurons to adapt to new tasks in continual learning settings (Yoon et al., 2018). The primary goal of these methods is to find an optimal network architecture or to adapt to new data distributions.

My Lifecycle principle differs from network growth in two fundamental ways. First, the motivation is different. I use dynamic structural changes for regularization within a fixed-capacity architecture,

not for finding a better architecture or expanding capacity. Second, and more critically, the mechanism is different. Network growth methods add brand new neurons that are randomly initialized. In contrast, my LC mechanism revives a specific, previously existing neuron. The revival process is guided by state memory, restoring the neuron to a previously useful state. This distinction is central to my work’s goal of maintaining training stability while still benefiting from dynamic network structures.

3 METHODOLOGY

In this section, I first explain the high-level concept of the Lifecycle (LC) principle. Then, I detail its specific implementation in a fully connected layer, which I call Lifecycle Linear (LCL).

3.1 THE LIFECYCLE PRINCIPLE

The Lifecycle principle is a dynamic regularization mechanism. It operates in three main stages for each individual neuron: Deactivation, State Memory, and Revival. The process is vividly shown in Figure 1.

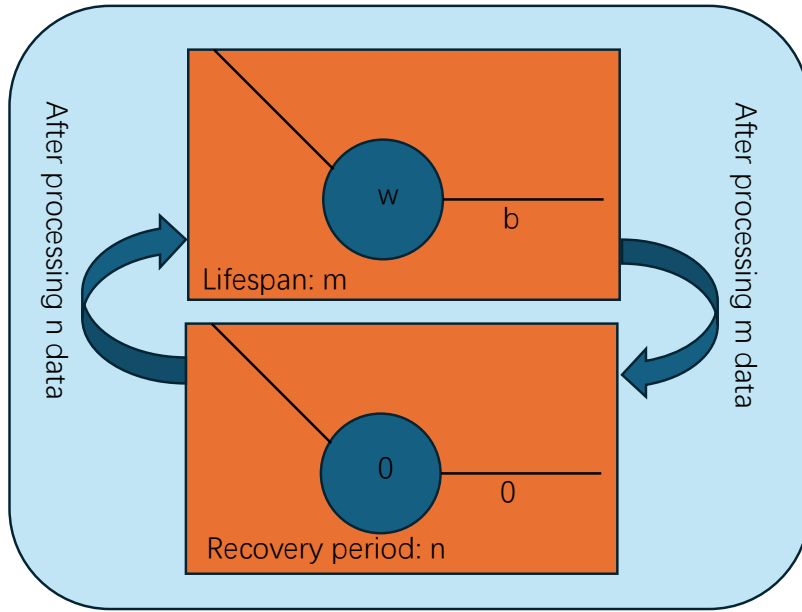


Figure 1: Diagram of the three stages of the Lifecycle principle

3.1.1 DEACTIVATION

Each neuron in a Lifecycle layer is assigned a random lifespan, measured in training steps. I sample this lifespan from a predefined range. A counter for each neuron tracks its remaining life. When the counter reaches zero, the neuron becomes inactive. It stops contributing to the network’s forward and backward passes.

3.1.2 STATE MEMORY

This is the core component of my principle. At the exact moment a neuron is deactivated, I save its current weight and bias parameters. These saved parameters are stored in separate, non-trainable buffers. The original parameters of the deactivated neuron remain in the network but do not receive any gradient updates, as their contribution is masked to zero.

3.1.3 REVIVAL

After deactivation, the neuron enters a recovery period. This period is also randomly sampled from a predefined range. When the recovery period ends, the neuron is revived. Upon revival, the neuron does not use random new weights. Instead, it restores the parameters that were saved in its state memory. This memory-aware process allows the neuron to return to a previously useful state.

3.2 INSTANTIATION ON FULLY CONNECTED LAYERS

I implemented the LC principle in a fully connected layer called Lifecycle Linear. This layer maintains several state buffers to manage the lifecycle of each neuron, including counters and the state memory buffers.

The layer uses an "is active" buffer as a binary mask during the forward pass. I multiply the layer's weights and biases by this mask. This effectively removes inactive neurons from the computation graph. As a result, no gradients flow to their parameters, and their weights are frozen.

As I discussed, re-initializing a revived neuron creates a large shock to the optimization. My state memory mechanism directly solves this problem. By restoring the neuron to its last known effective state, the revival process becomes a much smaller, non-destructive perturbation. My ablation studies in the experiments section will show that this memory component is critical for success.

To further smooth the revival process, I introduce a warm-up mechanism. When a neuron is revived, its output contribution is gradually scaled up to its full strength over a predefined number of training steps. I implement this with a "warmup scaler" buffer. This ensures the re-introduction of a neuron is a gradual and stable process. The detailed update steps are provided in Algorithm 1.

4 EXPERIMENT

In this section, I describe the experimental setup I used to evaluate the Lifecycle principle. I detail the datasets, the specific methods I compare, and the evaluation metrics. The goal is to empirically validate the effectiveness of my proposed mechanism.

4.1 DATASETS AND MODELS

I conducted experiments across a range of datasets and model architectures. For training from scratch, I used the CIFAR-10 and CIFAR-100 datasets (Krizhevsky & Hinton, 2009). I chose these because they are standard benchmarks for evaluating regularization methods. I used three different model architectures to test for generality. These were ResNet-18 (He et al., 2015), a convolutional network, DeiT-Tiny (Touvron et al., 2021), a vision transformer, and EfficientNetV2-S (Tan & Le, 2021), a modern efficient architecture. The results are shown in Table 1 and Table 2 respectively.

4.2 COMPARED METHODS

I compared my method, which I call LCL, against a comprehensive set of baseline and advanced regularization techniques. The Baseline method is a standard training setup without any specific regularization beyond what is in the base architecture. I also compared against weight decay (Krogh & Hertz, 1992), Dropout (Srivastava et al., 2014), DropConnect (Wan et al., 2013), Scheduled Drop, Label Smoothing (Szegedy et al., 2016), Stochastic Depth (Huang et al., 2016), and RigL (Evci et al., 2020). This wide range of competitors allows for a thorough evaluation of LCL's performance.

To understand the importance of each component of my method, I performed extensive Ablation Studies. I tested variants of LCL where the state memory was replaced with standard re-initialization schemes, which I call LCL-Reinit-He and LCL-Reinit-Xavier. I also tested versions of both the main method and the re-initialization variants without the warm-up mechanism, which I call LCL-no-warmup. These ablations are crucial for demonstrating that state memory is the key to stabilizing the training process.

4.3 EVALUATION METRICS

I used several metrics to evaluate the performance of each method. The primary metric is the final test accuracy (ACC), averaged over multiple runs. To assess robustness, I measured the mean accuracy on corrupted data (mCA) using the CIFAR-C benchmarks (Hendrycks & Dietterich, 2019). I also measured the Expected Calibration Error (ECE) to evaluate model confidence.

To connect my experimental results with my theoretical analysis, I measured two additional indicators. I estimated the sharpness of the loss minimum by computing the top eigenvalue of the Hessian matrix. I also computed a proxy for model capacity by calculating the product of the spectral norms of the network’s layers, which I call the Lipschitz bound.

Table 1: Performance comparison of various methods under different architectures on CIFAR-10

Model	Method	ACCURACY (%)	mCA (%)	ECE	Hessian top eigenvalue	Lipschitz bound
DeiT-Tiny	Baseline	82.28 ± 0.31	67.03 ± 0.70	0.1362 ± 0.0017	$2.5451 \times 10^{-02} \pm 2.1602 \times 10^{+02}$	$1.5915 \times 10^{+42} \pm 2.6503 \times 10^{+41}$
	DropConnect	77.68 ± 1.22	64.43 ± 1.24	0.1465 ± 0.0004	$2.2523 \times 10^{+00} \pm 2.4048 \times 10^{-01}$	$8.5564 \times 10^{+43} \pm 7.2450 \times 10^{+41}$
	Dropout	82.21 ± 0.71	66.82 ± 0.50	0.1387 ± 0.0046	$1.5750 \times 10^{-01} \pm 2.6088 \times 10^{-01}$	$1.1411 \times 10^{+43} \pm 1.9081 \times 10^{+42}$
	LCL	83.33 ± 0.55	66.76 ± 0.83	0.1310 ± 0.0032	$2.6858 \times 10^{-02} \pm 3.2738 \times 10^{-02}$	$1.1062 \times 10^{+18} \pm 7.6617 \times 10^{+17}$
	LCL-Reinit-He	83.60 ± 0.05	65.90 ± 0.90	0.0805 ± 0.0017	$2.2110 \times 10^{+00} \pm 1.4923 \times 10^{+00}$	$1.6676 \times 10^{+17} \pm 1.9316 \times 10^{+16}$
	LCL-Reinit-Xavier	80.29 ± 0.09	66.27 ± 1.11	0.0816 ± 0.0005	$2.0244 \times 10^{+00} \pm 4.0499 \times 10^{-01}$	$1.4175 \times 10^{+16} \pm 2.3110 \times 10^{+16}$
	LCL-no-warmup	79.46 ± 0.14	65.54 ± 0.24	0.0856 ± 0.0001	$5.8844 \times 10^{+00} \pm 4.1765 \times 10^{+00}$	$1.4066 \times 10^{+18} \pm 1.1204 \times 10^{+18}$
	LCL-Reinit-Xavier-no-warmup	79.65 ± 0.58	65.95 ± 0.30	0.0578 ± 0.0185	$6.5402 \times 10^{+00} \pm 8.8834 \times 10^{+00}$	$9.8294 \times 10^{+17} \pm 5.1318 \times 10^{+17}$
	LCL-no-warmup	82.46 ± 0.37	66.78 ± 0.24	0.1363 ± 0.0023	$7.1095 \times 10^{-03} \pm 4.9323 \times 10^{-03}$	$7.2936 \times 10^{+17} \pm 2.9854 \times 10^{+16}$
	Label Smoothing	82.69 ± 0.23	67.39 ± 0.78	0.0451 ± 0.0023	$6.3037 \times 10^{-01} \pm 5.3099 \times 10^{-01}$	$1.0906 \times 10^{+42} \pm 6.0460 \times 10^{+41}$
EfficientNetV2-S	RigL	80.43 ± 0.51	66.56 ± 0.62	0.1307 ± 0.0032	$3.8986 \times 10^{+00} \pm 6.3824 \times 10^{+00}$	$1.5706 \times 10^{+37} \pm 1.3807 \times 10^{+37}$
	Scheduled Drop	81.37 ± 0.21	66.75 ± 0.34	0.0937 ± 0.0125	$2.9252 \times 10^{+00} \pm 3.3648 \times 10^{+00}$	$4.8767 \times 10^{+44} \pm 4.9011 \times 10^{+44}$
	Stochastic Depth	82.74 ± 0.60	67.39 ± 0.49	0.1225 ± 0.0070	$1.2431 \times 10^{-01} \pm 1.3613 \times 10^{-01}$	$4.6156 \times 10^{+42} \pm 3.8933 \times 10^{+42}$
	Weight Decay	82.51 ± 0.16	67.24 ± 0.51	0.1318 ± 0.0048	$2.6994 \times 10^{-01} \pm 1.0701 \times 10^{-01}$	$1.3318 \times 10^{+42} \pm 1.1462 \times 10^{+42}$
	Baseline	91.75 ± 0.05	72.05 ± 0.39	0.0645 ± 0.0004	$6.2794 \times 10^{-01} \pm 1.6461 \times 10^{-01}$	$7.5175 \times 10^{-22} \pm 9.8524 \times 10^{-22}$
	DropConnect	91.95 ± 0.24	70.75 ± 0.41	0.0665 ± 0.0012	$3.9553 \times 10^{-01} \pm 8.6014 \times 10^{-01}$	$1.6440 \times 10^{-20} \pm 2.3193 \times 10^{-20}$
	Dropout	91.59 ± 0.27	69.96 ± 0.69	0.0652 ± 0.0009	$1.7330 \times 10^{-02} \pm 2.1141 \times 10^{-02}$	$2.9213 \times 10^{-21} \pm 6.9083 \times 10^{-21}$
	LCL	92.27 ± 0.23	70.76 ± 0.17	0.0631 ± 0.0022	$1.0894 \times 10^{-02} \pm 1.1036 \times 10^{+02}$	$3.5958 \times 10^{-23} \pm 6.1396 \times 10^{-23}$
	LCL-Reinit-He	91.83 ± 0.29	70.84 ± 0.30	0.0576 ± 0.0012	$7.5834 \times 10^{+00} \pm 8.8675 \times 10^{+00}$	$2.3634 \times 10^{-23} \pm 2.3656 \times 10^{-23}$
	LCL-Reinit-He-no-warmup	91.85 ± 0.11	70.67 ± 0.55	0.0587 ± 0.0032	$2.4284 \times 10^{-01} \pm 1.4831 \times 10^{+01}$	$1.0385 \times 10^{-22} \pm 1.5956 \times 10^{-22}$
ResNet-18	LCL-Reinit-Xavier	92.18 ± 0.17	71.59 ± 0.47	0.0543 ± 0.0044	$4.5209 \times 10^{+01} \pm 1.4300 \times 10^{+01}$	$1.2075 \times 10^{-23} \pm 1.4580 \times 10^{-23}$
	LCL-Reinit-Xavier-no-warmup	91.76 ± 0.11	70.51 ± 0.57	0.0597 ± 0.0045	$7.5225 \times 10^{-01} \pm 9.4649 \times 10^{+01}$	$5.5504 \times 10^{-23} \pm 2.1454 \times 10^{-23}$
	LCL-no-warmup	91.99 ± 0.12	70.86 ± 1.04	0.0631 ± 0.0023	$2.6111 \times 10^{+01} \pm 4.4439 \times 10^{+01}$	$3.3241 \times 10^{-23} \pm 4.0754 \times 10^{-23}$
	Label Smoothing	91.74 ± 0.09	71.12 ± 1.03	0.0643 ± 0.0019	$6.5665 \times 10^{+00} \pm 8.1441 \times 10^{+00}$	$6.7736 \times 10^{-19} \pm 8.2336 \times 10^{-19}$
	RigL	89.52 ± 0.39	68.05 ± 0.28	0.0700 ± 0.0047	$1.0623 \times 10^{+02} \pm 1.2399 \times 10^{+02}$	$6.5993 \times 10^{-11} \pm 9.6405 \times 10^{-11}$
	Scheduled Drop	91.68 ± 0.09	70.68 ± 0.37	0.0653 ± 0.0022	$1.3636 \times 10^{+00} \pm 2.2324 \times 10^{+00}$	$1.8530 \times 10^{-21} \pm 1.7848 \times 10^{-21}$
	Stochastic Depth	92.40 ± 0.09	71.58 ± 0.40	0.0557 ± 0.0006	$1.3775 \times 10^{-01} \pm 2.0836 \times 10^{+01}$	$2.4586 \times 10^{-21} \pm 3.2792 \times 10^{-21}$
	Weight Decay	91.50 ± 0.34	71.22 ± 1.04	0.0631 ± 0.0022	$1.0439 \times 10^{-01} \pm 1.8077 \times 10^{-01}$	$1.4272 \times 10^{-22} \pm 2.0451 \times 10^{-22}$
	Baseline	93.43 ± 0.36	75.21 ± 4.77	0.0526 ± 0.0005	$4.9701 \times 10^{-02} \pm 4.1458 \times 10^{-02}$	$2.2214 \times 10^{-01} \pm 1.4510 \times 10^{-01}$
	DropConnect	71.89 ± 17.52	60.49 ± 18.94	0.2332 ± 0.1451	$1.3182 \times 10^{-01} \pm 2.0798 \times 10^{-01}$	$4.2358 \times 10^{-01} \pm 7.7402 \times 10^{-01}$
EfficientNetV2-M	Dropout	93.54 ± 0.64	75.50 ± 5.04	0.0491 ± 0.0044	$1.1349 \times 10^{-01} \pm 6.1725 \times 10^{-02}$	$1.0360 \times 10^{+00} \pm 3.3019 \times 10^{-01}$
	LCL	94.19 ± 0.44	76.25 ± 4.67	0.0535 ± 0.0036	$3.2529 \times 10^{-02} \pm 6.6334 \times 10^{-02}$	$1.0329 \times 10^{-01} \pm 1.1494 \times 10^{-01}$
	LCL-Reinit-He	93.14 ± 0.41	75.38 ± 4.14	0.0533 ± 0.0057	$2.3166 \times 10^{-02} \pm 2.6333 \times 10^{-01}$	$7.9345 \times 10^{-02} \pm 7.9420 \times 10^{-02}$
	LCL-Reinit-He-no-warmup	93.14 ± 0.60	75.15 ± 4.35	0.0505 ± 0.0069	$2.6973 \times 10^{-01} \pm 2.3331 \times 10^{-01}$	$1.1790 \times 10^{-01} \pm 1.4865 \times 10^{-01}$
	LCL-Reinit-Xavier	93.20 ± 0.59	75.24 ± 3.93	0.0507 ± 0.0103	$7.7093 \times 10^{-01} \pm 6.4969 \times 10^{-01}$	$6.5194 \times 10^{-02} \pm 7.2337 \times 10^{-02}$
	LCL-Reinit-Xavier-no-warmup	93.26 ± 0.27	75.14 ± 3.96	0.0498 ± 0.0055	$5.7553 \times 10^{-01} \pm 9.3336 \times 10^{-01}$	$9.6476 \times 10^{-02} \pm 9.6587 \times 10^{-02}$
	LCL-no-warmup	93.21 ± 0.73	75.54 ± 4.99	0.0552 ± 0.0055	$1.0463 \times 10^{-01} \pm 1.4658 \times 10^{-01}$	$1.1077 \times 10^{-01} \pm 1.4656 \times 10^{-01}$
	Label Smoothing	93.50 ± 0.72	75.75 ± 4.51	0.0741 ± 0.0088	$5.2853 \times 10^{-03} \pm 3.9109 \times 10^{-00}$	$3.1636 \times 10^{-01} \pm 1.2444 \times 10^{-01}$
	RigL	92.66 ± 1.37	74.33 ± 2.97	0.0578 ± 0.0099	$5.6551 \times 10^{-03} \pm 1.8701 \times 10^{-03}$	$1.3246 \times 10^{+00} \pm 2.0818 \times 10^{+00}$
	Scheduled Drop	93.29 ± 0.71	74.88 ± 4.60	0.0627 ± 0.0057	$2.0393 \times 10^{-03} \pm 3.4935 \times 10^{-01}$	$8.6192 \times 10^{-01} \pm 9.2442 \times 10^{-01}$
ResNet-21	Stochastic Depth	93.64 ± 0.62	75.31 ± 4.04	0.0528 ± 0.0029	$4.2677 \times 10^{-03} \pm 1.3851 \times 10^{-01}$	$9.5992 \times 10^{-01} \pm 1.9771 \times 10^{-01}$
	Weight Decay	93.55 ± 0.55	75.25 ± 5.04	0.0484 ± 0.0045	$4.1750 \times 10^{-01} \pm 6.1375 \times 10^{-01}$	$2.2161 \times 10^{-01} \pm 2.2131 \times 10^{-01}$

For large-scale evaluation, I performed linear probing on the ImageNet-1k dataset (Russakovsky et al., 2015). For this, I used powerful pretrained models, including Swin Transformer (Liu et al., 2021), a model pre-trained on ImageNet-22k (Wightman, 2019); MambaOut-Base-Plus (Yu & Wang, 2024), a model pre-trained on ImageNet12k (Wightman, 2019); and EfficientNetV2-M (Tan & Le, 2021), a model pre-trained on ImageNet21k (Wightman, 2019). I froze their backbones and trained only the final classification layer. The final results are shown in Table 3.

Table 2: Performance comparison of various methods under different architectures on CIFAR-100

Model	Method	ACCURACY (%)	mCA (%)	ECE	Hessian top eigenvalue	Lipschitz bound
DeiT-Tiny	Baseline	54.01 \pm 0.58	38.67 \pm 0.44	0.3379 \pm 0.0026	$1.3948 \times 10^{-01} \pm 1.9338 \times 10^{-01}$	$4.7242 \times 10^{+42} \pm 7.1152 \times 10^{+42}$
	DropConnect	51.08 \pm 0.69	36.95 \pm 0.26	0.3262 \pm 0.0065	$1.7482 \times 10^{-01} \pm 3.2530 \times 10^{-02}$	$1.9420 \times 10^{+43} \pm 3.2222 \times 10^{+43}$
	Dropout	53.59 \pm 0.51	38.00 \pm 0.28	0.3481 \pm 0.0018	$2.0531 \times 10^{-03} \pm 3.4067 \times 10^{-03}$	$1.0061 \times 10^{+43} \pm 2.1348 \times 10^{+43}$
	LCL	54.43 \pm 0.24	37.72 \pm 0.44	0.2744 \pm 0.0324	$5.5074 \times 10^{-02} \pm 4.8620 \times 10^{-02}$	$6.9541 \times 10^{+16} \pm 1.4663 \times 10^{+16}$
	LCL-Reinit-He	53.83 \pm 0.34	38.98 \pm 0.33	0.1633 \pm 0.0018	$1.9306 \times 10^{-00} \pm 2.2615 \times 10^{-01}$	$1.3616 \times 10^{+16} \pm 2.1533 \times 10^{+15}$
	LCL-Reinit-Xavier	52.54 \pm 0.47	38.23 \pm 0.14	0.1793 \pm 0.0074	$3.4606 \times 10^{+00} \pm 1.7941 \times 10^{+00}$	$2.2845 \times 10^{+16} \pm 2.1903 \times 10^{+15}$
	LCL-no-warmup	52.33 \pm 0.18	37.65 \pm 0.77	0.1516 \pm 0.0167	$7.6328 \times 10^{-00} \pm 4.4879 \times 10^{+00}$	$1.3006 \times 10^{-17} \pm 3.1906 \times 10^{+17}$
	LCL-Reinit-Xavier-no-warmup	52.30 \pm 0.26	37.95 \pm 0.25	0.1306 \pm 0.0064	$7.9331 \times 10^{-00} \pm 5.3944 \times 10^{+00}$	$1.3514 \times 10^{-17} \pm 5.1344 \times 10^{+17}$
	LCL-no-warmup	55.11 \pm 0.37	38.85 \pm 0.71	0.3106 \pm 0.0064	$2.1349 \times 10^{-02} \pm 3.1156 \times 10^{-02}$	$1.1329 \times 10^{-17} \pm 6.2936 \times 10^{+16}$
	Label Smoothing	53.67 \pm 0.33	37.99 \pm 0.18	0.1392 \pm 0.0100	$1.7411 \times 10^{-02} \pm 1.1188 \times 10^{-02}$	$1.5658 \times 10^{+41} \pm 5.5770 \times 10^{+40}$
EfficientNetV2-S	RigL	53.20 \pm 0.72	37.78 \pm 0.36	0.3141 \pm 0.0015	$6.2725 \times 10^{-00} \pm 1.0343 \times 10^{+00}$	$1.3380 \times 10^{+40} \pm 1.0807 \times 10^{+40}$
	Scheduled Drop	52.37 \pm 0.47	37.83 \pm 0.24	0.1905 \pm 0.0359	$9.1753 \times 10^{-01} \pm 1.0371 \times 10^{+00}$	$3.9858 \times 10^{+42} \pm 2.6709 \times 10^{+42}$
	Stochastic Depth	54.24 \pm 0.26	39.19 \pm 0.05	0.3133 \pm 0.0050	$1.4656 \times 10^{-02} \pm 2.3980 \times 10^{-02}$	$2.5949 \times 10^{+42} \pm 3.5641 \times 10^{+42}$
	Weight Decay	54.81 \pm 0.41	38.48 \pm 0.08	0.3321 \pm 0.0025	$1.2025 \times 10^{-03} \pm 1.8803 \times 10^{-03}$	$1.6511 \times 10^{+42} \pm 9.2869 \times 10^{+41}$
	Baseline	57.21 \pm 0.73	38.56 \pm 1.51	0.3018 \pm 0.0020	$2.8125 \times 10^{-01} \pm 3.2802 \times 10^{-01}$	$1.0839 \times 10^{-10} \pm 1.1642 \times 10^{-10}$
	DropConnect	59.43 \pm 1.89	39.36 \pm 1.43	0.3107 \pm 0.0110	$1.1974 \times 10^{-03} \pm 1.7876 \times 10^{+03}$	$3.6018 \times 10^{-12} \pm 1.3731 \times 10^{-10}$
	Dropout	56.54 \pm 0.39	37.76 \pm 1.08	0.3048 \pm 0.0013	$2.2126 \times 10^{-02} \pm 2.6759 \times 10^{-02}$	$3.5782 \times 10^{-11} \pm 4.7974 \times 10^{-11}$
	LCL	58.15 \pm 0.23	37.18 \pm 2.55	0.2645 \pm 0.0464	$5.3978 \times 10^{-01} \pm 3.5875 \times 10^{-01}$	$3.6100 \times 10^{-12} \pm 2.3642 \times 10^{-12}$
	LCL-Reinit-He	56.45 \pm 0.50	37.84 \pm 0.60	0.1910 \pm 0.0657	$4.5453 \times 10^{-02} \pm 7.6228 \times 10^{+02}$	$1.2214 \times 10^{-11} \pm 1.5044 \times 10^{-11}$
	LCL-Reinit-He-no-warmup	56.42 \pm 1.13	37.39 \pm 1.01	0.1890 \pm 0.0534	$2.7878 \times 10^{-01} \pm 8.0738 \times 10^{-00}$	$2.0783 \times 10^{-12} \pm 1.9727 \times 10^{-12}$
ResNet-18	LCL-Reinit-Xavier	52.35 \pm 0.41	37.17 \pm 0.52	0.2212 \pm 0.0477	$2.1988 \times 10^{-01} \pm 5.1241 \times 10^{+01}$	$8.8096 \times 10^{-12} \pm 1.1389 \times 10^{-11}$
	LCL-Reinit-Xavier-no-warmup	57.35 \pm 0.41	37.89 \pm 1.22	0.2300 \pm 0.0485	$2.6606 \times 10^{-02} \pm 6.0844 \times 10^{+01}$	$5.2928 \times 10^{-12} \pm 5.0175 \times 10^{-12}$
	LCL-no-warmup	55.39 \pm 0.86	37.09 \pm 0.22	0.2296 \pm 0.0096	$3.1364 \times 10^{-01} \pm 1.8614 \times 10^{+01}$	$2.8765 \times 10^{-12} \pm 2.6846 \times 10^{-12}$
	Label Smoothing	57.45 \pm 0.64	38.62 \pm 1.12	0.1459 \pm 0.0130	$2.5083 \times 10^{-02} \pm 2.1937 \times 10^{-02}$	$2.8466 \times 10^{-12} \pm 9.3446 \times 10^{-13}$
	RigL	56.83 \pm 0.28	38.94 \pm 0.61	0.2999 \pm 0.0033	$2.1972 \times 10^{-02} \pm 2.5705 \times 10^{-02}$	$1.7599 \times 10^{-02} \pm 6.9873 \times 10^{-03}$
	Scheduled Drop	57.82 \pm 1.33	38.21 \pm 0.99	0.2976 \pm 0.0082	$1.6301 \times 10^{-02} \pm 1.7914 \times 10^{-02}$	$2.4043 \times 10^{-11} \pm 2.0662 \times 10^{-11}$
	Stochastic Depth	60.50 \pm 0.29	40.16 \pm 0.66	0.2703 \pm 0.0005	$5.4342 \times 10^{-02} \pm 5.0990 \times 10^{-02}$	$9.8176 \times 10^{-11} \pm 5.7824 \times 10^{-11}$
	Weight Decay	57.32 \pm 1.38	37.96 \pm 1.48	0.3018 \pm 0.0071	$9.1484 \times 10^{-03} \pm 1.1856 \times 10^{-02}$	$6.5511 \times 10^{-12} \pm 3.2157 \times 10^{-12}$
	Baseline	72.37 \pm 0.72	48.36 \pm 4.14	0.1977 \pm 0.0037	$1.0278 \times 10^{+01} \pm 1.7300 \times 10^{+01}$	$8.3905 \times 10^{+01} \pm 1.4533 \times 10^{+01}$
	DropConnect	31.99 \pm 29.20	26.68 \pm 24.57	0.3050 \pm 0.2158	$4.4670 \times 10^{-01} \pm 8.0806 \times 10^{-01}$	$1.1637 \times 10^{+01} \pm 1.0594 \times 10^{+02}$
MambaOut-Base-Plus	Dropout	71.61 \pm 2.03	48.34 \pm 4.35	0.1941 \pm 0.0071	$1.0858 \times 10^{+01} \pm 9.7259 \times 10^{+00}$	$1.6117 \times 10^{+02} \pm 3.0594 \times 10^{+02}$
	LCL	73.66 \pm 1.71	45.47 \pm 1.64	0.1912 \pm 0.0127	$3.6664 \times 10^{-01} \pm 2.2816 \times 10^{-01}$	$1.3910 \times 10^{+00} \pm 1.1327 \times 10^{-01}$
	LCL-Reinit-He	71.66 \pm 2.72	47.34 \pm 2.68	0.1602 \pm 0.0052	$3.8145 \times 10^{-01} \pm 5.4406 \times 10^{+01}$	$2.5190 \times 10^{+00} \pm 2.6940 \times 10^{-01}$
	LCL-Reinit-He-no-warmup	71.39 \pm 1.63	47.56 \pm 3.37	0.1336 \pm 0.0080	$1.6174 \times 10^{-01} \pm 2.2813 \times 10^{+01}$	$3.9836 \times 10^{+00} \pm 4.6940 \times 10^{-01}$
	LCL-Reinit-Xavier	71.34 \pm 1.20	47.19 \pm 3.84	0.1733 \pm 0.0114	$1.1861 \times 10^{-01} \pm 8.0830 \times 10^{+01}$	$5.3008 \times 10^{+00} \pm 1.2632 \times 10^{+00}$
	LCL-Reinit-Xavier-no-warmup	71.14 \pm 1.68	47.35 \pm 4.24	0.1722 \pm 0.0089	$2.1038 \times 10^{-01} \pm 2.0787 \times 10^{+01}$	$1.9828 \times 10^{+00} \pm 2.6232 \times 10^{+00}$
	LCL-no-warmup	71.78 \pm 2.83	48.10 \pm 2.41	0.1951 \pm 0.0065	$3.9850 \times 10^{-01} \pm 5.0949 \times 10^{-01}$	$2.3778 \times 10^{-01} \pm 3.0159 \times 10^{-01}$
	Label Smoothing	74.83 \pm 2.24	51.51 \pm 2.51	0.0870 \pm 0.0331	$1.9374 \times 10^{-00} \pm 4.4046 \times 10^{-01}$	$8.9299 \times 10^{-00} \pm 9.7109 \times 10^{-01}$
	RigL	69.80 \pm 3.59	46.30 \pm 0.81	0.2169 \pm 0.0191	$2.9351 \times 10^{-00} \pm 3.3243 \times 10^{+00}$	$1.3993 \times 10^{-01} \pm 2.3572 \times 10^{+01}$
	Scheduled Drop	70.70 \pm 1.97	47.13 \pm 4.09	0.2034 \pm 0.0055	$3.5669 \times 10^{-01} \pm 4.0958 \times 10^{+01}$	$5.6291 \times 10^{-01} \pm 1.6187 \times 10^{+02}$
Swin Transformers Base	Stochastic Depth	72.08 \pm 1.61	47.60 \pm 4.02	0.1863 \pm 0.0023	$8.4402 \times 10^{-01} \pm 3.3872 \times 10^{-01}$	$1.1387 \times 10^{-02} \pm 5.2736 \times 10^{-01}$
	Weight Decay	72.39 \pm 1.72	48.61 \pm 3.65	0.1985 \pm 0.0066	$8.2750 \times 10^{+00} \pm 5.5200 \times 10^{+00}$	$1.0977 \times 10^{+01} \pm 7.7622 \times 10^{+00}$

Table 3: Performance comparison of various methods under different architectures on ImageNet1k

Model	Method	ACCURACY (%)	ECE	Hessian top eigenvalue	Lipschitz bound
EfficientNetV2-M	Baseline	79.21 \pm 0.25	0.0653 \pm 0.0331	$1.1966 \times 10^{+00} \pm 4.1874 \times 10^{-01}$	$1.1555 \times 10^{-69} \pm 2.9840 \times 10^{-70}$
	Drop Connect	79.88 \pm 0.21	0.0901 \pm 0.0229	$1.1788 \times 10^{+00} \pm 9.9937 \times 10^{-01}$	$1.6893 \times 10^{-69} \pm 6.2454 \times 10^{-70}$
	Dropout	80.60 \pm 0.11	0.0673 \pm 0.0005	$7.0280 \times 10^{-01} \pm 3.5335 \times 10^{-01}$	$1.2979 \times 10^{-69} \pm 8.0208 \times 10^{-73}$
	LCL	79.47 \pm 0.16	0.0267 \pm 0.0026	$7.3600 \times 10^{-01} \pm 3.7410 \times 10^{-01}$	$4.5327 \times 10^{-71} \pm 0.0000 \times 10^{+00}$
	Label Smoothing	80.51 \pm 0.05	0.1152 \pm 0.0049	$3.1510 \times 10^{-01} \pm 3.4629 \times 10^{-02}$	$7.3717 \times 10^{-70} \pm 1.2501 \times 10^{-72}$
	Weight Decay	79.14 \pm 0.39	0.0662 \pm 0.0346	$1.6910 \times 10^{+00} \pm 7.8445 \times 10^{-01}$	$1.1547 \times 10^{-69} \pm 3.0004 \times 10^{-70}$
MambaOut-Base-Plus	Baseline	84.76 \pm 0.03	0.0272 \pm 0.0006	$6.6450 \times 10^{-06} \pm 4.1953 \times 10^{-06}$	$1.6666 \times 10^{-06} \pm 3.6373 \times 10^{-09}$
	Drop Connect	84.77 \pm 0.21	0.0379 \pm 0.0008	$5.3900 \times 10^{-06} \pm 3.2147 \times 10^{-06}$	$1.6364 \times 10^{-06} \pm 1.3299 \times 10^{-08}$
	Dropout	84.84 \pm 0.05	0.0281 \pm 0.0003	$7.6089 \times 10^{-04} \pm 1.3173 \times 10^{-03}$	$1.6719 \times 10^{-06} \pm 3.2747 \times 10^{-09}$
	LCL	84.92 \pm 0.08	0.0445 \pm 0.0097	$1.4567 \times 10^{-04} \pm 2.0020 \times 10^{-04}$	$5.0834 \times 10^{-08} \pm 2.8868 \times 10^{-12}$
	Label Smoothing	84.78 \pm 0.05	0.0272 \pm 0.0006	$6.0973 \times 10^{-05} \pm 4.2399 \times 10^{-05}$	$1.4985 \times 10^{-06} \pm 7.5498 \times 10^{-10}$
Swin Transformers Base	Weight Decay	84.83 \pm 0.01	0.0276 \pm 0.0003	$2.1959 \times 10^{-05} \pm 1.5427 \times 10^{-05}$	$1.6736 \times 10^{-06} \pm 1.6166 \times 10^{-09}$
	Baseline	83.32 \pm 0.04	0.0199 \pm 0.0002	$2.3857 \times 10^{-05} \pm 3.0471 \times 10^{-05}$	$1.5562 \times 10^{+79} \pm 1.5133 \times 10^{+76}$
	Drop Connect	83.23 \pm 0.03	0.0699 \pm 0.0137	$5.3240 \times 10^{-06} \pm 5.4957 \times 10^{-06}$	$2.3201 \times 10^{+79} \pm 5.1445 \times 10^{+78}$
	Dropout	83.18 \pm 0.07	0.0203 \pm 0.0003	$4.4510 \times 10^{-05} \pm 4.3814 \times 10^{-05}$	$1.5553 \times 10^{+79} \pm 1.2702 \times 10^{+76}$
	LCL	83.58 \pm 0.07	0.0204 \pm 0.0002	$1.6853 \times 10^{-04} \pm 2.8892 \times 10^{-04}$	$1.9846 \times 10^{+78} \pm 0.0000 \times 10^{+00}$
Swin Transformers Base	Label Smoothing	82.91 \pm 0.05	0.0869 \pm 0.0004	$1.6841 \times 10^{-04} \pm 1.9370 \times 10^{-04}$	$1.4611 \times 10^{+79} \pm 5.6226 \times 10^{+76}$
	Weight Decay	83.22 \pm 0.07	0.0208 \pm 0.0005	$2.7792 \times 10^{-06} \pm 4.5940 \times 10^{-06}$	$1.5557 \times 10^{+79} \pm 3.6116 \times 10^{+76}$

5 THEORETICAL ANALYSIS

In this section, I provide a theoretical analysis of the Lifecycle (LC) principle. My goal is to explain why this mechanism can act as an effective regularizer. I formalize the training objective under the LC principle. Then, I show that this process favors solutions with lower curvature and reduced model capacity. My analysis directly connects to the empirical metrics I will present in the experiments section.

5.1 FORMALIZING THE TRAINING OBJECTIVE

I view the LC principle as a process of applying a stochastic, memory-aware mask to the network’s parameters. For a network f_{θ} and a training set $\mathbb{S} = \{(\mathbf{x}_i, \mathbf{y}_i)\}_{i=1}^n$, the standard empirical risk is:

$$\mathcal{L}(\theta) = \frac{1}{n} \sum_{i=1}^n \ell(f_{\theta}(\mathbf{x}_i), \mathbf{y}_i). \quad (1)$$

For a Lifecycle Linear layer, the forward pass uses a dynamic mask vector $\mathbf{d}_t \in [0, 1]^m$, where m is the number of output neurons. The output is equivalent to

$$\mathbf{y} = (\mathbf{W} \odot \mathbf{D}_t) \mathbf{x} + (\mathbf{b} \odot \mathbf{d}_t), \quad \text{where } \mathbf{D}_t = \text{diag}(\mathbf{d}_t), \quad \mathbf{d}_t \in [0, 1]^m. \quad (2)$$

The vector \mathbf{d}_t is determined by the lifecycle process. It is 0 for inactive neurons, 1 for fully active neurons, and between (0,1) for neurons in their warm-up phase.

Let \mathbf{M}_t represent the collective mask for all LC layers at step t . The training process can be seen as optimizing the parameters θ under this sequence of random masks. I define the smoothed training objective $\bar{\mathcal{L}}(\theta)$ as the expected loss over the stationary distribution \mathcal{P} of the masks:

$$\bar{\mathcal{L}}(\theta) = \mathbb{E}_{\mathbf{M} \sim \mathcal{P}} \left[\frac{1}{n} \sum_{i=1}^n \ell(f_{\theta \odot \mathbf{M}}(\mathbf{x}_i), \mathbf{y}_i) \right]. \quad (3)$$

This smoothed objective represents the average loss over a family of subnetworks generated by the lifecycle process. The state memory component does not change this objective. Instead, it stabilizes the optimization path towards a minimum of this objective, which I confirm in my ablation studies.

5.2 CONCLUSION A: SMOOTHING THE LOSS LANDSCAPE AND FAVORING FLAT MINIMA

The LC mechanism optimizes a smoothed version of the original loss function. This smoothing has a direct effect on the curvature of the loss landscape.

Proposition 1. *According to the Equation 3, the Hessian of the smoothed objective $\bar{\mathcal{L}}(\theta)$ is an expectation over the Hessians of the masked objectives. Assume that ℓ is quadratically differentiable and that the exchange of expectation and derivative is legal (which is valid under finite samples and bounded gradients). Then:*

$$\nabla_{\theta}^2 \bar{\mathcal{L}}(\theta) = \mathbb{E}_{\mathbf{M} \sim \mathcal{P}} [\text{Diag}(\mathbf{M}) \nabla_{\theta}^2 \mathcal{L}(\theta \odot \mathbf{M}) \text{Diag}(\mathbf{M})].$$

This means the masking process attenuates the curvature. The maximum eigenvalue of the smoothed Hessian is bounded by the maximum eigenvalue of the original Hessian. This suggests that the optimizer is guided towards flatter minima. Prior work has established a strong connection between flat minima and better generalization performance (Keskar et al., 2017).

Proposition 2. *In the neighborhood of θ , let the mask be $\mathbf{M} = \mathbf{1} - \xi$, where $\xi \in [0, 1]^d$ indicates a slight weakening of the multiplication. We perform a second-order Taylor expansion on $\mathcal{L}(\theta \odot \mathbf{M}) = \mathcal{L}(\theta \odot (\mathbf{1} - \xi))$ and take the expectation. If the gradient vanishes at θ (i.e., $\nabla_{\theta} \mathcal{L}(\theta) = 0$), then the smoothed objective is approximately:*

$$\bar{\mathcal{L}}(\theta) \approx \mathcal{L}(\theta) + \frac{1}{2} \sum_{i=1}^d \text{Var}[\xi_i] \theta_i^T (\nabla_{\theta}^2 \mathcal{L}(\theta)) \theta_i.$$

The second term on the right is a curvature-weighted "ridge" penalty: the greater the curvature (sharp minima), represented by $\nabla_{\theta}^2 \mathcal{L}(\theta)$, or the larger the coordinate magnitude, $\|\theta\|^2$, the more $\bar{\mathcal{L}}$ penalizes it. Unlike ordinary ridge regression, $\lambda \|\theta\|_2^2$, this penalty is adaptively weighted by the Hessian, forming a "curvature-aware ridge".

I empirically validate this proposition. I use the top eigenvalue of the Hessian matrix to measure the sharpness of the final solution and use power iteration to estimate this eigenvalue. My theory predicts that the LCL-trained model exhibits significantly lower top eigenvalues of the Hessian matrix compared to the baseline model. This is demonstrated in Tables 1, 2 and 3.

5.3 CONCLUSION B: REDUCING MODEL CAPACITY FOR BETTER GENERALIZATION

The LC mechanism also acts as a form of capacity control. It reduces the expected complexity of the function class that the network can represent. This can be analyzed through the network's Lipschitz constant.

Proposition 3. *The expected Lipschitz constant of a network with LC layers is contracted. For an L -layer network with 1-Lipschitz activations, the expected Lipschitz constant is bounded by:*

$$\mathbb{E}_M [\text{Lip}(f_{\theta \odot M})] \leq \left(\prod_{\ell=1}^L \mu_\ell \right) \cdot \prod_{\ell=1}^L \|\mathbf{W}^{(\ell)}\|_2.$$

Here, $\|\mathbf{W}^{(\ell)}\|_2$ is the spectral norm of the weight matrix of layer ℓ . The factor $\mu_\ell = \sqrt{\mathbb{E}[(\mathbf{d}^{(\ell)})^2]} \in (0, 1]$ is less than 1 because neurons are inactive or warming up for a fraction of the time. A smaller Lipschitz constant implies a smaller Rademacher complexity of the function class (Bartlett & Mendelson, 2002). This leads to a tighter generalization bound.

Let $\mathcal{F}_{\text{base}}$ be the class of functions without LCL, and \mathcal{F}_{LCL} be the class of functions with random masking (independent of the data), then the empirical Rademacher complexity satisfies:

$$\hat{\mathfrak{R}}_n(\mathcal{F}_{\text{LCL}}) \lesssim \left(\prod_{\ell=1}^L \mu_\ell \right) \cdot \hat{\mathfrak{R}}_n(\mathcal{F}_{\text{base}}), \quad (4)$$

Thus, the generalization error bound is tightened:

$$\mathbb{E}[\text{gen_gap}] \lesssim \tilde{O} \left(\left(\prod_{\ell=1}^L \mu_\ell \right) \cdot \frac{\prod_{\ell=1}^L \|\mathbf{W}^{(\ell)}\|_2 \cdot \text{diam}(\mathcal{X})}{\sqrt{n}} \right). \quad (5)$$

That is, the greater the masking strength (the smaller μ_ℓ), the tighter the generalization upper bound.

I provide evidence for this capacity reduction. I compute a proxy for the network's Lipschitz constant by multiplying the spectral norms of its layers' weight matrices. My theory predicts that the LCL-trained model achieves strong performance while maintaining a smaller Lipschitz constant proxy compared to the baseline. This is demonstrated in Tables 1, 2 and 3.

5.4 CONCLUSION C: REDUCING CO-ADAPTATION

Proposition 4. *Under the first-order necessary conditions of $\bar{\mathcal{L}}$,*

$$\mathbb{E}_M [\mathbf{M} \odot \nabla_{\theta} \mathcal{L}(\theta \odot \mathbf{M})] = 0.$$

Because $\mathbb{P}[d_i = 0] > 0$ for each coordinate i , this condition forces the overall target to remain stationary even when any single neuron is absent with a certain probability—this is equivalent to weakening the reliance on individual neurons/connections. This is similar to the "ensemble effect" of dropout, but LCL is stronger: the absence is "long-windowed" (lifetime length) rather than instantaneous and random on a sample-by-sample basis, thus more substantially suppressing co-adaptation.

Proposition 5. *Assume that \mathcal{L} has a large Hessian eigenvalue in the direction of the principal curvature of a sharp minimum θ^\ddagger . If $\text{Var}[d_i] > 0$ and the warm-up is such that $d_i \in (0, 1)$ within the*

non-ignored fraction of training, then according to Proposition 2, under the second-order approximation of θ^\sharp , the additional term introduced by $\bar{\mathcal{L}}$ in this direction is $\frac{1}{2}\text{Var}[d_i] \cdot \theta_i^\top H(\theta^\sharp)\theta_i$, and its magnitude increases linearly with the curvature. Therefore, θ^\sharp is often not a minimum of $\bar{\mathcal{L}}$ (or its basin becomes significantly shallower/narrower). Under LCL, the scheduler is less likely to be “locked” by the sharp basin and tends to shift to flatter regions.

The reduction in co-adaptation leads to improved robustness. I verify this by evaluating the final model’s performance on corrupted test sets, such as CIFAR-10-C (Hendrycks & Dietterich, 2019). My theory predicts that the LCL-trained model demonstrates higher accuracy on these datasets, indicating that it has learned more robust features.

6 CONCLUSION

In this paper, I introduced the Lifecycle (LC) principle, a new regularization mechanism for training neural networks. The core idea is to let individual neurons undergo long-term cycles of deactivation and revival. I identified that this dynamic process can cause training instability. To address this, I proposed a state memory component as the key part of my method. This component allows a revived neuron to restore its previously learned parameters, which effectively mitigates optimization shocks.

My theoretical analysis suggests that the LC principle smooths the loss landscape and encourages the optimizer to find flatter minima. My experiments show that my implementation, Lifecycle Linear, improves generalization and robustness over standard baselines. The results also confirm that state memory is critical for the method’s success.

The Lifecycle principle is a general concept. In this work, I only applied it to fully connected layers. An important direction for future research is to extend this principle to other architectures. For example, one could apply it to the channels of convolutional neural networks or to the attention heads in Transformers (Vaswani et al., 2017). Exploring how the Lifecycle principle interacts with different model types is a promising area for future work.

REFERENCES

Peter L Bartlett and Shahar Mendelson. Rademacher and gaussian complexities: Risk bounds and structural results. *Journal of Machine Learning Research*, 3(Nov):463–482, 2002.

Davis Blalock, Jose Javier Gonzalez Ortiz, Jonathan Frankle, and John Guttag. What is the state of neural network pruning? In *Proceedings of machine learning and systems*, volume 2, pp. 129–146, 2020.

Tianqi Chen, Ian Goodfellow, and Jonathon Shlens. Net2net: Accelerating learning via knowledge transfer. *arXiv preprint arXiv:1511.05641*, 2015.

Utku Evci, Trevor Gale, Jacob Menick, Pablo Samuel Castro, and Erich Elsen. Rigging the lottery: Making all tickets winners. In *International conference on machine learning*, pp. 2943–2952. PMLR, 2020.

Song Han, Jeff Pool, John Tran, and William J. Dally. Learning both weights and connections for efficient neural networks. In *Proceedings of the 29th International Conference on Neural Information Processing Systems - Volume 1*, NIPS’15, pp. 1135–1143, Cambridge, MA, USA, 2015. MIT Press.

Kaiming He, Xiangyu Zhang, Shaoqing Ren, and Jian Sun. Deep residual learning for image recognition. *arXiv preprint arXiv:1512.03385*, 2015.

Dan Hendrycks and Thomas Dietterich. Benchmarking neural network robustness to common corruptions and perturbations. In *International Conference on Learning Representations*, 2019. URL <https://openreview.net/forum?id=HJz6ticqYm>.

Gao Huang, Yu Sun, Zhuang Liu, Derek Sedra, and Kilian Q Weinberger. Deep networks with stochastic depth. *European Conference on Computer Vision*, 2016.

Nitish Shirish Keskar, Dheevatsa Mudigere, Jorge Nocedal, Mikhail Smelyanskiy, and Ping Tak Peter Tang. On large-batch training for deep learning: Generalization gap and sharp minima. In *International Conference on Learning Representations*, 2017. URL <https://openreview.net/forum?id=H1oyR1Ygg>.

Alex Krizhevsky and Geoffrey Hinton. Learning multiple layers of features from tiny images. *Master's thesis, University of Toronto*, 2009.

Anders Krogh and John Hertz. Avoiding overfitting. *Neural Computation*, 4(2):220–226, 1992.

Ze Liu, Yutong Lin, Yue Cao, Han Hu, Yixuan Wei, Zheng Zhang, Stephen Lin, and Baining Guo. Swin transformer: Hierarchical vision transformer using shifted windows. In *Proceedings of the IEEE/CVF International Conference on Computer Vision (ICCV)*, 2021.

Decebal C Mocanu, Elena Mocanu, Peter Stone, Phu H Nguyen, Madeleine Gibescu, and Antonio Liotta. Scalable training of artificial neural networks with adaptive sparse connectivity inspired by network science. *Nature communications*, 9(1):2383, 2018.

Olga Russakovsky, Jia Deng, Hao Su, Jonathan Krause, Sanjeev Satheesh, Sean Ma, Zhiheng Huang, Andrej Karpathy, Aditya Khosla, Michael Bernstein, Alexander C. Berg, and Li Fei-Fei. ImageNet Large Scale Visual Recognition Challenge. *International Journal of Computer Vision (IJCV)*, 115(3):211–252, 2015. doi: 10.1007/s11263-015-0816-y.

Nitish Srivastava, Geoffrey Hinton, Alex Krizhevsky, Ilya Sutskever, and Ruslan Salakhutdinov. Dropout: a simple way to prevent neural networks from overfitting. *J. Mach. Learn. Res.*, 15(1):1929–1958, January 2014. ISSN 1532-4435.

Christian Szegedy, Vincent Vanhoucke, Sergey Ioffe, Jon Shlens, and Zbigniew Wojna. Rethinking the inception architecture for computer vision. *arXiv preprint arXiv:1512.00567*, 2016.

Mingxing Tan and Quoc Le. Efficientnetv2: Smaller models and faster training. In *International conference on machine learning*, pp. 10096–10106. PMLR, 2021.

Hugo Touvron, Matthieu Cord, Matthijs Douze, Francisco Massa, Alexandre Sablayrolles, and Hervé Jegou. Training data-efficient image transformers & distillation through attention. In *International Conference on Machine Learning*, volume 139, pp. 10347–10357, July 2021.

Ashish Vaswani, Noam Shazeer, Niki Parmar, Jakob Uszkoreit, Llion Jones, Aidan N Gomez, Łukasz Kaiser, and Illia Polosukhin. Attention is all you need. In I. Guyon, U. Von Luxburg, S. Bengio, H. Wallach, R. Fergus, S. Vishwanathan, and R. Garnett (eds.), *Advances in Neural Information Processing Systems*, volume 30. Curran Associates, Inc., 2017. URL https://proceedings.neurips.cc/paper_files/paper/2017/file/3f5ee243547dee91fb053c1c4a845aa-Paper.pdf.

Li Wan, Matthew Zeiler, Sixin Zhang, Yann Le Cun, and Rob Fergus. Regularization of neural networks using dropconnect. In Sanjoy Dasgupta and David McAllester (eds.), *Proceedings of the 30th International Conference on Machine Learning*, volume 28 of *Proceedings of Machine Learning Research*, pp. 1058–1066, Atlanta, Georgia, USA, 17–19 Jun 2013. PMLR. URL <https://proceedings.mlr.press/v28/wan13.html>.

Ross Wightman. Pytorch image models. <https://github.com/huggingface/pytorch-image-models>, 2019.

Jaehong Yoon, Eunho Yang, Jeongtae Lee, and Sung Ju Hwang. Lifelong learning with dynamically expandable networks. In *International Conference on Learning Representations*, 2018. URL <https://openreview.net/forum?id=Sk7KsfW0->.

Weihao Yu and Xinchao Wang. Mambaout: Do we really need mamba for vision? *arXiv preprint arXiv:2405.07992*, 2024.

A ALGORITHM

Algorithm 1 Lifecycle Linear Update Step

Require: Weights $W \in \mathbb{R}^{m \times d}$, Bias $b \in \mathbb{R}^m$; Memory buffers $W^{\text{mem}} \in \mathbb{R}^{m \times d}$, $b^{\text{mem}} \in \mathbb{R}^m$; State buffers: activity mask $a \in \{0, 1\}^m$, warm-up scaler $s \in [0, 1]^m$, life counters $c^{\text{life}} \in \mathbb{R}^m$, recovery counters $c^{\text{rec}} \in \mathbb{R}^m$; Hyperparameters: max durations $L_{\text{max}} \in \mathbb{R}^m$, $R_{\text{max}} \in \mathbb{R}^m$, warm-up steps $k \in \mathbb{N}_+$.

```

1: procedure INITIALIZE
2:    $a \leftarrow \mathbf{1}$ ;  $s \leftarrow \mathbf{1}$ ;  $c^{\text{rec}} \leftarrow \mathbf{0}$ 
3:    $c_i^{\text{life}} \sim U[l_{\text{min}}, l_{\text{max}}]$  for  $i = 1, \dots, m$ 
4:    $W^{\text{mem}} \leftarrow W$ ;  $b^{\text{mem}} \leftarrow b$ 
5: end procedure

6: if not in training mode then return                                 $\triangleright$  Lifecycle updates only occur during training.
7: end if
    $\triangleright$  (A) Warm-up Phase: Ramp up recently revived neurons
8:  $I_{\text{warm-up}} \leftarrow \{i \mid s_i < 1\}$                                  $\triangleright$  Perfectly matches the Python code.
9:  $s_{I_{\text{warm-up}}} \leftarrow \min(1, s_{I_{\text{warm-up}}} + 1/k)$ 
    $\triangleright$  (B) Update Timers
10:  $c^{\text{life}} \leftarrow c^{\text{life}} - a$ 
11:  $c^{\text{rec}} \leftarrow c^{\text{rec}} - (1 - a)$ 
    $\triangleright$  (C) Lysis Phase: Deactivate expired neurons
12:  $I_{\text{lyse}} \leftarrow \{i \mid a_i = 1 \wedge c_i^{\text{life}} \leq 0\}$ 
13: if  $I_{\text{lyse}} \neq \emptyset$  then                                          $\triangleright$  Save parameters to memory.
14:    $W^{\text{mem}}[I_{\text{lyse}}, :] \leftarrow W[I_{\text{lyse}}, :]$ 
15:    $b^{\text{mem}}[I_{\text{lyse}}] \leftarrow b[I_{\text{lyse}}]$ 
16:    $a_{I_{\text{lyse}}} \leftarrow 0$ 
17:    $c_{I_{\text{lyse}}}^{\text{rec}} \leftarrow R_{\text{max}, I_{\text{lyse}}}$ 
18:    $s_{I_{\text{lyse}}} \leftarrow 1$                                           $\triangleright$  Reset scaler for the next revival.
19: end if
    $\triangleright$  (D) Revival Phase: Reactivate recovered neurons
20:  $I_{\text{revive}} \leftarrow \{i \mid a_i = 0 \wedge c_i^{\text{rec}} \leq 0\}$ 
21: if  $I_{\text{revive}} \neq \emptyset$  then                                          $\triangleright$  Restore from memory.
22:    $W[I_{\text{revive}}, :] \leftarrow W^{\text{mem}}[I_{\text{revive}}, :]$ 
23:    $b[I_{\text{revive}}] \leftarrow b^{\text{mem}}[I_{\text{revive}}]$ 
24:    $a_{I_{\text{revive}}} \leftarrow 1$ 
25:    $c_{I_{\text{revive}}}^{\text{life}} \leftarrow L_{\text{max}, I_{\text{revive}}}$ 
26:    $s_{I_{\text{revive}}} \leftarrow 1/k$                                           $\triangleright$  Initiate warm-up.
27: end if

```

B HYPERPARAMETERS

Table 4: Key hyperparameters in CIFAR-10 and CIFAR-100 training configurations.

Category	Parameter	Value
Dataset	Validation Split	10% of the training data
Training Dynamics	Epochs	100
	Batch Size	128
	Loss Function	Cross-Entropy Loss (except for the Label Smoothing experiment)
	Random Seeds	42, 123, 888 (3 separate runs)
Optimizer	Optimizer	AdamW ($\beta_1 = 0.9, \beta_2 = 0.999$)
	Learning Rate (LR)	1×10^{-3}
	LR Scheduler	Warmup Cosine Decay
	Warmup Epochs	5
Data Augmentation	Transformations	RandomCrop, RandomHorizontalFlip
	Normalization	The mean and standard deviation of the data set

Table 5: Key hyperparameters in ImageNet-1k training configurations.

Category	Parameter	Value
Dataset	Validation Split	10% of the training data
Training Dynamics	Epochs	15
	Batch Size	256
	accumulation	32
	Loss Function	Cross-Entropy Loss (except for the Label Smoothing experiment)
	Random Seeds	42, 123, 888 (3 separate runs)
Optimizer	Optimizer	AdamW ($\beta_1 = 0.9, \beta_2 = 0.999$)
	Learning Rate (LR)	1×10^{-2}
	LR Scheduler	Warmup Cosine Decay
	Warmup Epochs	5
Data Augmentation	Transformations	RandomCrop, RandomHorizontalFlip
	Normalization	The mean and standard deviation of the data set